# Vestigial like 4 regulates the adipogenesis of classical brown adipose tissue

Runing title: VGLL4 regulates brown adipose tissue development

Pingzhu Zhou[a, *, &], Chase W. Kessinger[b, *], Fei Gu[a], Amanda Davenport[b], Genyu Wang[b], Steven G. Negron[b], Bart Deplancke[c], William T. Pu[a], Zhiqiang Lin[b, #].

a. Boston Children's Hospital, 300 Longwood Ave, Boston, MA, 02115

b. Department of Biomedical Research and Translational Medicine, Masonic Medical Research Institute, 2150 Bleecker St, Utica, NY 13501

c. Swiss Institute of Bioinformatics, CH-1015 Lausanne, Switzerland

&. Current affiliation: Shanghai 411 Hospital, School of Medicine, Shanghai University, 99 Shangda Road, Shanghai, 200444, China.

*P. Z. and C.W.K contributed equally to this work.

[#] To whom correspondence should be addressed: zlin@mmri.edu

## Abstract

Brown adipose tissue (BAT) is mammals' primary non-shivering thermogenesis organ, and the molecular mechanisms regulating BAT growth and adipogenesis are largely unknown. The Hippo-YAP pathway has been well-known for controlling organ size, and Vestigial like 4 (VGLL4) is a transcriptional regulator that modulates the Hippo-YAP pathway by competing against YAP for binding to TEAD proteins. In this study, we dissected the function of VGLL4 in regulating BAT development. We generated a conventional *Vgll4* mutant mouse line, in which the two Tondu (TDU) domains of VGLL4 were disrupted. We found that deletion of the TDU domains of VGLL4 resulted in perinatal lethality and paucity of the interscapular BAT. Histological and magnetic resonance imaging studies confirmed that the adipogenesis of BAT was impaired in *Vgll4* mutants. Adeno-associated virus (AAV) mediated, brown adipocyte-specific overexpression of VGLL4 increased BAT volume and protected the adult male mice from acute cold stress. Genomic studies suggest that VGLL4/TEAD1 complex directly regulates the myogenic and adipogenic gene expression programs of BAT. In conclusion, our data identify VGLL4 as a previously unrecognized adipogenesis factor that regulates classical BAT development.

**Keywords:** Vestigial like 4, TEAD1, CEBPβ, Hippo-YAP pathway, classical brown adipose tissue, development, adipogenesis.

## 1. Introduction

Obesity is a global epidemic that contributes to a number of chronic disease conditions, such as type 2 diabetes mellitus, non-alcoholic fatty liver, cardiovascular disease, and cancers (Mitchell et al., 2011). In mammals, the adipose tissue comprises white and brown adipose tissue (WAT and BAT, respectively) (Zwick et al., 2018). WAT stores triglycerides in adipocytes, and its expansion is a hallmark of obesity. On the other hand, BAT burns triglycerides and glucose to generate heat (Symonds, 2013). Based on its developmental origin, BAT is further divided into classical BAT and white adipocyte-derived brown adipocytes (beige/brite cells) (Giralt and Villarroya, 2013). In humans, BAT is abundant in infants, and decreases with age (Heaton, 1972). Recently, the discovery of functional BAT and beige cells in adults (Cypess et al., 2009) raises the possibility of treating obesity by activating BAT or increasing the browning of WAT (Cypess and Kahn, 2010). Thus understanding the molecular mechanisms that control BAT growth and function is critical for developing therapeutic strategies to treat obesity.

Both white adipocytes and classical brown adipocytes (BACs) are derived from mesenchymal stem cells (Gesta et al., 2007). BAC adipogenesis generally includes four steps. First, mesenchymal stem cells differentiate into myogenic factor 5 (Myf5)-expressing progenitor cells. Next, Myf5$^{+}$ progenitor cells differentiate into brown preadipocytes, which then differentiate into UCP1-positive naive BACs. Finally, naive BACs develop into lipid-loaded and mitochondria abundant mature BACs (Yao et al., 2011). In mice, the interscapular BAT depot appears at embryonic day 15.5 (E15.5), and expands rapidly during fetal and neonatal development. BAT lipogenesis is minimal in murine embryos and increases remarkably after birth (Schulz et al., 2013; Negron et al., 2020).

The genetic programs controlling BAT adipogenesis are well documented. Transcription

55 factors, including peroxisome proliferator-activated receptor gamma (PPARγ), CCAAT/
56 enhancer-binding proteins (specifically CEBPβ/δ), and PRD1-BF-1-RIZ1 homologous domain
57 containing protein-16 (PRDM16), are key regulators of BAC differentiation (Gesta et al., 2007;
58 Yao et al., 2011; Townsend and Tseng, 2012). Conditional deletion of *Pparg* in adipocytes
59 reduced both WAT and BAT (Jones et al., 2005). Mice missing both CEBPβ and CEBPδ had
60 no lipid accumulation in BAT, and primary embryonic fibroblasts lacking both of these factors
61 failed to undergo adipocyte differentiation (Tanaka et al., 1997). PRDM16 is a crucial regulator
62 of myogenic and brown adipogenic lineage differentiation, because ectopic expression of
63 PRDM16 in myoblasts activated the BAC differentiation program, which relied on the
64 interaction between PRDM16 and CEBPβ/δ (Seale et al., 2007).
65 The Hippo-YAP kinase signaling pathway is well known for controlling organ growth
66 (Pan, 2010). In mammals, upstream signaling pathways activate the Hippo kinase cascade,
67 comprised of MST1/2, LATS1/2, and the scaffold protein Salvador (Sav). Activation of this
68 kinase cascade results in phosphorylation and inactivation of YAP and WWTR1 (more
69 commonly referred to as TAZ), orthologous transcriptional co-activators that are terminal
70 transcriptional effectors of this pathway. YAP/TAZ interact with TEAD family transcription
71 factors to regulate downstream target gene expression, including genes that control cell
72 proliferation (Meng et al., 2016). Several studies have implicated Hippo-YAP signaling in WAT
73 adipogenesis. In the 3T3-L1 preadipocyte cell line, which has been widely used to study WAT
74 adipocyte differentiation (Morrison and McGee, 2015), overexpression or knock-down of
75 Hippo kinases activated or suppressed adipogenesis, respectively (Park et al., 2012; An et al.,
76 2013), while knock-down of YAP/TAZ or TEAD4 augmented WAT adipogenesis (Yu et al.,
77 2013; Zhang et al., 2018). YAP/TAZ-TEAD complex also plays an important role in regulating
78 BAT adipogenesis. BAT-specific YAP/TAZ double heterozygous mice (YTU) had reduced BAT
79 size and impaired metabolic activity at 4 weeks of age. At 20 weeks of age, compared with the
80 BAT of the age matched control mice, the YTU BAT was two times larger, which was due to

81 excessive lipid accumulation in the BACs (Tharp et al., 2018). However, the underlying
82 molecular mechanism of how YAP/TAZ-TEAD complex regulates BAT adipogenesis has not
83 been well documented.

84 In addition to inhibition by the Hippo kinase cascade, the activity of the YAP/TAZ-TEAD
85 complex is also suppressed by Vestigial like 4 (VGLL4), a transcriptional regulator that
86 competes with YAP/TAZ for binding to TEAD (Koontz et al., 2013; Lin et al., 2016). In 3T3-L1
87 cells, loss of either TEAD4 or VGLL4 increased adipogenesis; overexpressing TEAD4
88 suppressed adipogenesis, which was abolished by knocking down VGLL4 (Zhang et al.,
89 2018). These data highlight the importance of VGLL4 as a crucial regulator of adipogenesis in
90 vitro and raise the question whether VGLL4 regulates adipogenesis in vivo.

91 Previously, we generated a *Vgll4* mutant mouse allele, *Vgll4*$^{d46}$, in which a 46 bp deletion
92 caused a frameshift mutation and disrupted the TDU domain that mediates TEAD binding.
93 *Vgll4*$^{d46/d46}$ (*Vko*) mice could not prevail and died shortly after birth (Sheldon et al., 2022). Using
94 interscapular BAT as a classical BAT example, here we show that *Vko* mice had much less
95 BAT than their littermate controls, and that VGLL4 is essential for the normal BAT
96 adipogenesis gene expression program. Additionally, overexpressing VGLL4 in postnatal BAT
97 increased BAT volume and protected the mice from acute cold stress. In summary, our study
98 reveals that VGLL4 is a crucial adipogenesis factor that controls BAT growth and function,
99 thus advancing the knowledge of BAT development.

100 ***Results***

101 ***Mutating VGLL4 causes BAT paucity.***

102 We have previously reported that whole-body depletion of VGLL4 led to perinatal death
103 (Sheldon et al., 2022). While characterizing the phenotype of the *Vgll4* knockout (*Vko*) pups,
104 we noticed that the *Vko* newborn pups had consistent dents in the interscapular regions,

105 which led us to examine the interscapular BAT depot. Impressively, the *Vko* pups had much
106 smaller BAT depots than their littermate controls (Fig. 1A). By performing qRT-PCR with the
107 P0 BAT we confirmed the depletion of *Vgll4* (Suppl. Fig. 1A).

108 To elucidate the cellular mechanism of BAT paucity, we first examined the BAC size and
109 found reduced BAC size in *Vko* compared with littermate controls (Suppl. Fig. 1B and 1C).
110 We then measured the proliferation rate of the UCP1-positive BACs with EdU, a thymidine
111 analogue that labels proliferating cells. *Vko* BACs had a comparable EdU incorporation rate to
112 controls (Suppl. Fig. 2D and 2E). Consistent with the malformation of BAT, the expression of
113 BAT marker UCP1 was reduced in the *Vko* mutants (Fig. 1B and 1C), suggesting that loss of
114 VGLL4 may either interfere with preadipocyte-to-BAC differentiation or impair BAC
115 maturation.

116 To determine if the BAT abnormalities preceded birth, we collected embryos at E18.5 and
117 examined the interscapular BAT depot. Compared with wild type controls, the *Vgll4*
118 heterozygous (*Vhet*) embryos had no obvious growth defects, as reflected by the normal body
119 weight (Suppl. Fig. 1F). The *Vko* mutants were smaller than both wild type and *Vhet* embryos;
120 however, the weight of the major internal organs, such as the heart and lungs, normalized to
121 body weight, was not affected (Suppl. Fig. 1G and 1H). Because we observed no phenotypic
122 difference between *Vhet* and wild type mice, we used both of these genotypes as controls. In
123 the control embryos, the interscapular regions were filled with BAT covered by white
124 adipocytes (Suppl. Fig. 1I); however, the *Vko* embryos had much smaller interscapular BAT
125 depots (Suppl. Fig. 1I), demonstrating that BAT paucity occurs in *Vko* during embryonic
126 development.

127 We further examined the BAT histology and lipid deposition in the neonatal *Vko* mutants.
128 The BAT depot was thinner in *Vko* than in controls (Fig. 1D, top row). The nuclei were more
129 dense in *Vko* BAT, and *Vko* BACs had less cytoplasmic vacuoles (Fig. 1D, bottom row).

130 Oil Red O staining revealed that lipid droplets were abundant in control BAT but rarely

131 detected in the *Vko* BAT (Fig. 1E), suggesting that VGLL4 is essential for BAT lipogenesis.

132 Similar to BAT, the inguinal subcutaneous white adipose tissue (iWAT) contained minimal
133 lipid droplets in *Vko*, whereas lipid droplets were readily detected in control iWAT (Fig. 1F).
134 Perilipin is a protein enriched on the surface of lipid droplets in differentiated adipocytes
135 (Greenberg et al., 1991). Compared with control iWAT, *Vko* iWAT had much less perilipin
136 immunoreactivity (Fig. 1F). To more broadly assess the effect of VGLL4 mutation on lipid
137 deposition, we measured the lipid composition of the chest and abdomen of control and *Vko*
138 pups with magnetic resonance imaging (MRI). Lipid signals were detected in the interscapular
139 and subcutaneous regions of control but not *Vko* pups (Fig. 1G). Quantification of the relative
140 volume of BAT and subcutaneous WAT revealed that both these adipose depots were much
141 smaller in the *Vko* pups (Fig. 1H and 1I). Additionally, quantification of the lipid signals
142 contained in the chest and abdomen tissues demonstrated a significant decrease of lipid
143 content in the *Vko* mutants (Fig. 1J, *Vko* 1.49% vs Ctrl 19.59%, p=0.01). Together, these data
144 suggest that VGLL4 regulates adipogenesis in both BAT and subcutaneous WAT.

145 **Loss of VGLL4 disrupts the adipogenesis gene expression program of BAT.**

146 To determine whether VGLL4 inactivation changed the BAT gene expression program, we
147 performed RNA sequencing with BAT collected from P0 pups. Compared with littermate
148 controls, 1217 and 978 genes were significantly down- and up- regulated in the *Vko* BAT,
149 respectively ($P_{adj}$<0.05 and absolute FC>1.5; Fig. 2A, Supplemental table 1). Whole genome
150 Gene Set Enrichment Analysis (GESA) analysis (Subramanian et al., 2005) showed that
151 myogenesis, oxidative phosphorylation, fatty acid metabolism, and adipogenesis were the top
152 four biological processes enriched in the wild type BAT (Fig. 2B; Suppl. Fig.2A). Out of 191
153 genes in the adipogenesis gene set, 51 were down-regulated in *Vko* (Fig. 2C). We used qRT-
154 PCR to validate the expression of *Acsl1, Adipor2, Cidea* and *Dgat1,* and confirmed that all
155 these genes except *Adipor2* were decreased in *Vko* BAT (Fig. 2D).

156 To assess the BAC differentiation stage that is regulated by VGLL4, we took advantage of

157 published gene expression profiles of BACs at different stages of differentiation (Pradhan et
158 al., 2017). In this study, 960 protein coding genes were found to be differentially expressed
159 during pre-adipocyte to BAC differentiation. Among these 960 genes, 856 genes were
160 detected in our RNA-seq data. Based on the expression data of these 856 genes, we
161 performed hierarchical clustering to determine which stage of differentiation was most similar
162 to P0 control or *Vko* BAT. Both the control and *Vko* BAT gene expression data clustered with
163 that of the differentiated BACs (Suppl. Fig. 2B), suggestive a minor role of VGLL4 during
164 brown preadipocyte to BAC differentiation.

165 We further measured the expression of two BAC-enriched genes (*Ucp1* and *Cox7a1*) and
166 two BAC differentiation-related genes (*Dlk1/Pref-1* and *Prdm16*). In comparison with control
167 BAT, *Vko* BAT had lower expression of *Ucp1* and *Cox7a1* (Fig. 2E) and similar expression of
168 *Dlk1* and *Prdm16* (Fig. 2F).

169 ***Deletion of VGLL4 activates IGF-Akt pathway.***

170 VGLL4 is a transcriptional regulator that blunts the interaction between YAP and TEAD
171 proteins (Lin et al., 2016). It has been reported that mice doubly heterozygous for YAP and its
172 paralog TAZ had disrupted BAT growth, and that YAP/TAZ coordinated with TEAD1 to drive
173 UCP1 expression in BACs (Tharp et al., 2018). These published data suggest that TEAD1 is
174 involved in the development of BAT. To test the correlation between TEAD1 expression and
175 BAT development, we examined *Tead1* mRNA and TEAD1 protein levels in the BAT at
176 different developmental stages. *Tead1* mRNA and TEAD1 protein were both high in postnatal
177 day 1 (P1) BAT and then quickly decreased to a very low level at P4 (Fig. 3A; Suppl. Fig. 3A).
178 Different from *Tead1*, *Vgll4* mRNA level was decreased from P1 to P15 and then increased
179 from P15 to P30 (Supp. Fig. 3B).

180 We previously showed that activation of VGLL4 decreased TEAD1 protein level in the
181 heart (Lin et al., 2016) and knocking out VGLL4 increased TEAD1(Sheldon et al., 2022). We
182 then checked whether inactivation of VGLL4 affected TEAD1 protein expression in BAT.

183 Immunofluorescence staining showed that TEAD1 expression and nuclear abundance was
184 both increased in the BACs of neonatal *Vko* (Fig. 3B). In line with these in situ observations,
185 western blots confirmed that *Vko* BAT had more TEAD1 than littermate controls (Fig. 3C and
186 3D). The YAP/TEAD complex regulates the expression of IGFR-Akt pathway components (Xin
187 et al., 2011; Lin et al., 2015). Consistent with the upregulation of TEAD1, the *Vko* pups had
188 increased IGF1R and higher phospho Akt/Akt ratio (Fig. 3C and 3D). These data suggest that
189 VGLL4 ablation increases the transcriptional activity of the TEAD1/YAP complex in BAT.
190 Next, we measured the protein levels of PPAR-γ and CEBPβ, two transcriptional factors
191 central to the regulation of adipogenesis (Farmer, 2006; Guo et al., 2015). PPARγ was
192 significantly increased in *Vko* BAT (Fig. 3E and 3F ), suggesting that loss of VGLL4 does not
193 impair BAT adipogenesis by decreasing PPARγ expression. CEBPβ plays a central role in
194 adipocyte differentiation (Guo et al., 2015), and it has several N-terminally truncated isoforms,
195 such as liver-enriched activator protein (LAP) and liver-enriched inhibitory protein (LIP).
196 CEBPβ-LAP interacts with PRDM16 to direct the differentiation of myoblastic precursors into
197 BACs (Seale et al., 2009), and CEBPβ-LIP rescued the growth defects of *Cebpb* knockout
198 mice (Bégay et al., 2018), suggesting that CEBP-LIP and CEBP-LAP have overlapping
199 functions. Compared to control BAT, CEBPβ-LAP expression in *Vko* BAT was similar, but
200 CEBPβ-LIP was significantly lower (Fig. 3E and 3F).
201 Adipose triglyceride lipase (ATGL) is a well-known lipolysis enzyme and highly
202 expressed in the adipose tissues of mice and humans (Zimmermann et al., 2004). It recently
203 was shown to regulate the synthesis of branched fatty acid esters of hydroxy fatty acids
204 (FAHFAs) (Patel et al., 2022), a class of newly discovered lipids that have favorable metabolic
205 and anti-inflammatory effects (Yore et al., 2014). In *Vko* BAT, ATGL expression was very low
206 compared to control BAT (Fig. 3E and 3F), further suggesting that loss of VGLL4 impairs the
207 development of BAT.
208 **VGLL4/TEAD1 complex regulates the expression of BAT myogenesis genes.**

209 We suspected that VGLL4 might interact with TEAD1 to regulate BAC gene expression. To
210 test this hypothesis, we used a genomic approach to identify the genes that are regulated by
211 both VGLL4 and TEAD1.

212 Because TEAD1 expression was high in the young newborn pups (Fig. 3A), we used P0
213 BAT to identify genes directly bound by TEAD1 using TEAD1 chromatin immunoprecipitation
214 followed by next generation sequencing (ChIP seq). *Tead1*$^{fb}$ knockin mice that express FLAG
215 and BIO epitope tagged TEAD1 (Lin et al., 2016) were crossed to BirA transgenic
216 mice(Driegen et al., 2005) to generate *Tead1*$^{fb}$;*BirA* mice, in which the endogenous TEAD1$^{fb}$
217 protein was biotylated by BirA.

218 TEAD1 bioChIP-seq of P0 *Tead1*$^{fb}$*;BirA* BAT revealed 4234 peaks that mapped to 2834
219 genes, with 371 peaks localized in the promoter region (0 to -5kb upstream of the
220 transcriptional starting site), and the rest of the peaks spreading out in the gene bodies and
221 distal noncoding regions (Suppl. Fig. 4A). De novo motif discovery (Heinz et al., 2010)
222 identified the TEAD binding motif as the mostly enriched motif (Fig. 4A), thus confirming the
223 reliability of our ChIP seq data set. The other top five transcriptional factors that were co-
224 enriched in the TEAD1 ChIP peaks were Nuclear factor 1 (NF1), CCCTC-Binding Factor
225 (CTCF), CEBP, Early B Cell Factor transcription factor 1 (EBF1) and Myocyte Enhancer
226 Factor 2C (MEF2c) (Fig. 4A). Among these five transcriptional factors, both NF1 and CEBP
227 protein families are essential for BAT adipogenesis (Tanaka et al., 1997; Hiraike et al., 2017),
228 suggesting that TEAD1 may coordinate with these transcriptional factors to regulate BAT
229 development.

230 Pathway analysis with the 2834 TEAD1-bound genes showed that the Hippo signaling
231 pathway was among the top five enriched pathways (Fig. 4B). By comparing the *Vko* BAT
232 differentially regulated genes (DEG) with the TEAD1-bound genes, we identified 419
233 overlapped genes that might be directly regulated by VGLL4 and TEAD1 (Fig. 4C). Gene
234 ontology term analysis (Ge et al., 2020) of these 419 genes revealed that muscle structure

235 development was the most enriched biological process (Fig. 4D). 37 TEAD1-bound genes
236 were differentially expressed in *Vko* BAT and related to muscle structure development (Fig.
237 4E). Myogenic gene expression is a molecular signature that separates BACs from white
238 adipocytes (Timmons et al., 2007). These data suggest that the VGLL4/TEAD1 complex
239 regulates the expression of myogenic genes in BAT.

240 In addition to regulating myogenic genes, TEAD1 also bound to crucial lipogenesis genes,
241 such as *Fabp4, Lpl, Fabp3, Cd36, Prdm16, Cav1, Slc27a1,* and *Ppargc1b* (Suppl. Fig. 4B).
242 qRT-PCR tests confirmed that *Cav1*, *Fabp3*, *Slc27a1,* and *Ppargc1b* were all down regulated
243 in the *Vko* BAT (Suppl. Fig. 4C).

244 **VGLL4 alleviates TEAD1 suppression of CEBPβ transcriptional activity.**

245 Calsequestrin1 (*Casq1*) encodes a high-capacity calcium-binding protein that acts as a
246 $Ca^{2+}$ storage/buffer molecule in the sarcoplasmic reticulum of skeletal muscle cells (Sanchez
247 et al., 2012). *Casq1* is also expressed in BAT, and down regulation of *Casq1* is associated
248 with decreased BAT thermogenic capacity (Anthony et al., 2020). Unbiased *Vko* BAT gene
249 expression profiling and TEAD1 ChIP-seq analysis identified *Casq1* as a direct target of the
250 VGLL4/TEAD1 complex (Fig. 4E). As shown in Fig. 5A, TEAD1 directly bound to the promoter
251 region of *Casq1*. In BAT, *Vgll4* inactivation robustly decreased *Casq1* mRNA (Fig. 5B). TEAD1
252 ChIP-seq peak region encompassed 480 base pairs (bp) of the *Casq1* promoter. Analysis of
253 mouse and human sequences using the evolutionary conserved regions (ECR) genome
254 browser (Ovcharenko et al., 2004) showed that the sequence is highly conserved (Fig. 5C)
255 and contains one CEBP binding motif and one TEAD1 binding motif, both of which were
256 identical between mouse and human (Fig. 5D).

257 To study the activity of murine *Casq1* promoter, we constructed Casq1-Luci, in which the
258 480 bp TEAD1-bound region was positioned upstream of the luciferase gene in the
259 promoterless pGL2 basic vector (Fig. 5E). In HEK293T cells, CEBPβ increased Casq1-Luci
260 reporter activity, which was attenuated by further addition of TEAD1. VGLL4 did not affect

261 CEBPβ transcriptional activity, but it abolished TEAD1 suppression of CEBPβ (Fig. 5E).

262 We performed co-immunoprecipitation (Co-IP) assays in HEK293T cells to characterize
263 the relationships between CEBPβ, VGLL4, and TEAD1. Plasmids expressing TEAD1-HA,
264 VGLL4-GFP and CEBPB-FLAG were co-transfected into HEK293T cells in different
265 combinations. In the absence of TEAD1-HA, CEBPβ-FLAG pulled down VGLL4-GFP (Suppl.
266 Fig.5); in the absence of VGLL4-GFP, CEBPβ-FLAG pulled down TEAD1-HA (Fig. 5F). When
267 these three proteins were co-expressed in HEK293T cells, CEBPβ pulled down both VGLL4
268 and TEAD1 (Fig. 5F). These data suggest that TEAD1 and VGLL4 each bind to CEBPβ in a
269 non-exclusive manner.

270 Altogether, these data suggest that TEAD1 suppresses CEBPβ activation of *Casq1*
271 expression, and that VGLL4 favors *Casq1* expression by abolishing TEAD1 suppression of
272 CEBPβ.

273 **Construction and validation of a BAC-specific AAV construct.**

274 AAV-mediated transduction of adipose tissue is a convenient tool for studying adipose
275 pathophysiology, and AAV serotype 9 has a very high transduction efficiency for BAT
276 (Jimenez et al., 2013). To facilitate gene-function studies in BAT, we generated a new AAV
277 construct in which brown adipose tissue-specific cis-regulatory elements (BCE) derived from
278 murine *Ucp1* drive cargo gene expression (Suppl. Fig. 6). To test the specificity and activity of
279 BCE, we cloned either luciferase or GFP into this construct (Fig. 6A). 3-day-old pups (P3)
280 were treated with AAV9.BCE.Luci and AAV9.BCE.GFP. 6 weeks post AAV delivery, we
281 examined the tissue specificity of these AAV constructs (Fig. 6B). In vivo bioluminescence
282 imaging showed that luciferase activity was limited to the interscapular region (Fig. 6C).
283 Overlay of the luciferase signal onto whole animal microCT data confirmed that it originated
284 from BAT (Fig. 6D). Histological sections of interscapular adipose tissue confirmed that BCE-
285 driven GFP was expressed in BACs and not in the adjacent white adipocytes (Fig. 6E).

286 **Overexpressing VGLL4 in BACs promotes BAT growth.**

287 Because loss of VGLL4 caused BAT paucity (Fig. 1), we asked whether overexpressing
288 VGLL4 in BACs promotes BAT growth.

289 To answer this question we generated AAV.BCE.VGLL4$^{GFP}$ (BCE.VGLL4$^{GFP}$), in which
290 BAC-specific BCE regulatory elements drive the expression of GFP tagged human VGLL4.
291 We treated p3 pups with BCE.VGLL4$^{GFP}$ and assessed BAT volume at P42 using microCT
292 (Fig. 7A). BCE.GFP was used as a control. Compared with BCE.GFP treated mice,
293 BCE.VGLL4$^{GFP}$ mice showed significantly higher BAT volume (102.20 ± 2.77 vs 84.16 ± 1.86
294 mm$^3$, Fig. 7B), whereas the body weight of these two cohorts animals was not distinguishable
295 (Fig. 7C). Compared with BCE.GFP, BCE.VGLL4$^{GFP}$ treatment resulted in significantly higher
296 interscapular BAT volume (102.20 ± 2.76 vs 84.16 ± 1.86 mm$^3$, Fig. 8B), whereas the body
297 weight of these groups was indistinguishable (Fig. 7C). Consistent with the *microCT*
298 measurements, the BAT weight to body weight ratio was significantly higher for
299 BCE.VGLL4$^{GFP}$ compared to BCE.GFP (Fig. 7D).

300 We collected the BAT tissue to confirm the expression of VGLL4$^{GFP}$. Western blot
301 detected the expression of VGLL4$^{GFP}$ in the BCE.VGLL4$^{GFP}$ transduced mice (Fig. 7E), and in
302 situ immunofluorescence staining showed that VGLL4$^{GFP}$ signals were enriched in the nuclei
303 of BACs (Suppl. Fig. 7A).

304 Because lipogenesis-driven BAC enlargement is one of the underlying mechanisms of
305 postnatal BAT growth (Negron et al., 2020), we suspected that VGLL4 might promote BAT
306 growth by increasing BAC size. We tested this hypothesis by staining BAT sections with
307 Phalloidin, which labels the filamentous actin cytoskeleton (Kim et al., 2019). Compared to
308 BCE.GFP, BCE.VGLL4$^{GFP}$ significantly increased BAC size (Suppl. Fig. 7B and 7C), which
309 was associated with the increase of lipid content as visualized by BODIPY ( a neutral lipid
310 dye) staining (Suppl. Fig. 7D and 7E). To corroborate the in vivo results, we overexpressed
311 VGLL4 in an immortalized brown preadipocyte (IBA) cell line (Pradhan et al., 2017) and tested
312 VGLL4's adiogenetic effects. Compared with GFP control, VGLL4 promoted lipid deposition in

313 differentiated IBA cells (Suppl. Fig. 7F). Correspondingly, qRT-PCR results demonstrated the
314 robust increase of three lipogenesis genes: *Fasn*, *Cidea* and *Acsl1* (Suppl. Fig. 7G). Thus, our
315 in vitro and in vivo data strongly suggest that activation of VGLL4 promotes BAT growth by
316 increasing BAC lipogenesis.

317 Thermogenesis is one of the biological functions of BAT. We asked whether activating
318 VGLL4 in BAT affected whole body thermogenesis. To address this issue, we transduced P3
319 wild type mouse pups with BCE.VGLL4$^{GFP}$ and performed acute cold stress test 6 weeks post
320 AAV transduction. Age-matched BCE.GFP transduced mice were used as control.
321 BCE.VGLL4$^{GFP}$ and BCE.GFP mice were applied to acute 4°C cold stress for 24 hours. The
322 core temperature of these two cohorts of mice were indistinguishable under regular housing
323 temperature (~22 °C). In the first 20-hour acute cold stress period, the core temperature of
324 male BCE.GFP mice decreased from 37.10 $\pm$ 0.21 °C to 35.28 $\pm$ 0.72 °C; however, the core
325 temperature of the male BCE.VGLL4$^{GFP}$ mice did not change (37.43 $\pm$ 1.15 vs 37.80 $\pm$ 0.62)
326 (Fig. 7F). In contrast to the male mice, the female mice did not show a core temperature
327 difference between BCE.GFP and BCE.VGLL4$^{GFP}$ groups (Fig. 7G).

328 On the molecular level, we collected BAT after acute cold stress and measured the
329 expression of several VGLL4/TEAD1 target genes, including *Casq1, Myh9, Smad6,* and
330 *Tpm1.* qRT-PCR results showed that VGLL4 increased *Casq1* and decreased *Smad6* (Fig.
331 7H). In line with our observation that VGLL4 promoted lipogenesis, *Cidea* expression was
332 increased in BCE.VGLL4$^{GFP}$ BAT. Although VGLL4 activation increased BAT thermogenesis,
333 we found that VGLL4 decreased *Ucp1* expression, rather than increasing it (Fig. 7H).

334 **Discussion**

335 In this study, we found that germ-line deletion of the VGLL4 TDU domains impaired BAT
336 growth. Our data suggest that BAT adipogenesis requires VGLL4.

337 From fetus to early life, the development of BACs encompasses four stages: 1)
338 mesenchymal stem cells differentiate into myogenic factor 5 (Myf5)-expressing progenitor

339 cells; 2) Myf5$^{+}$ progenitor cells differentiate into brown preadipocytes; 3) preadipocytes
340 differentiate into UCP1-positive naive BACs; 4) naive BACs develop into lipid-loaded and
341 mitochondria abundant mature BACs (Yao et al., 2011). Our current data advocate the
342 hypothesis that VGLL4 regulates BAT growth by orchestrating molecular events that occur
343 between stage 3 and 4, a developmental period required for brown preadipocytes turning into
344 lipid-loaded and thermogenesis active mature BACs. This hypothesis is supported by the
345 following data sets: first, loss of VGLL4 impairs BAC lipogenesis and UCP1 expression;
346 second, the *Vko* BAT gene expression signature was more similar to the differentiated BACs
347 than the undifferentiated brown preadipocytes; third, VGLL4 gain-of-function studies show
348 that activating VGLL4 increased BAT volume and BAC size; fourth, VGLL4 promotes
349 lipogenesis in cultured BACs.

350 We found that VGLL4 promotes both BAT and WAT lipogenesis *in vivo*. This result differs
351 from studies performed in cultured 3T3L1 cells, which suggested that VGLL4 suppresses
352 adipogenesis (Zhang et al., 2018). One possibility is that under physiological conditions,
353 VGLL4 is essential for orchestrating the lipogenesis of adipocytes. However, under harsh
354 chemical adipogenesis conditions, such as the chemical cocktail for inducing 3T3L1 cells
355 differentiation into adipocytes, VGLL4 may be required to block the excessive activity of the
356 adipogenesis factors.

357 Akt signaling is pivotal for BAT development, because genetically ablation of Akt1 and
358 Akt2 severely diminished BAT growth (Shearin et al., 2016). In the neonatal *Vko* BAT, the
359 expression of TEAD1, IGFR and phospho-Akt were all increased, suggestive of VGLL4
360 impairing BAT development without blunting Akt pathway. PPARγ and CEBPβ are two master
361 regulators of adipogenesis (Tanaka et al., 1997; Jones et al., 2005; Xiong et al., 2018). In
362 rodents, CEBPβ-LIP is abundant in fetal BAT and low in adult BAT(Manchado et al., 1994),
363 and expressing CEBPβ-LIP in the CEBPβ knockout mice rescued BAT adipogenesis(Bégay et
364 al., 2018), implying that CEBPβ-LIP is critical for BAT development. In *Vko* BAT, PPARγ was

365 increased, whereas the expression of two CEBPβ isoforms was differentially regulated, with
366 the larger CEBPβ-LAP isoform remaining unchanged and the smaller CEBPβ-LIP isoform
367 being substantially reduced.

368 As VGLL4's partner and one of the terminal effectors of Hippo-YAP pathway, TEAD1 is
369 highly expressed in the P1 BAT and its expression decreases with age. In P0 BAT, TEAD1
370 bound regions are enriched with CEBP binding motif, suggestive of TEAD1 and CEBP
371 collaborative binding. Using the murine *Casq1* promoter that contains conserved TEAD1 and
372 CEBP binding motifs as a probe, we found that CEBPβ activated *Casq1* expression whereas
373 adding in TEAD1 weakened CEBPβ's transcriptional activity. This TEAD1 suppression of
374 CEBPβ is likely a direct regulation due to direct protein-protein interactions, because co-IP
375 experiments indicate that these proteins interact with each other. VGLL4 is known to
376 physically interact with TEAD1, and here we show that VGLL4 also interacts with CEBPβ.
377 Although VGLL4 did not affect CEBPβ transcriptional activity, it abolished TEAD1 suppression
378 of CEBPβ. The discovery of VGLL4 alleviating TEAD1 suppression of CEBPβ, together with
379 the aforementioned *Vko* BAT signaling pathways profiling data suggest that VGLL4 and
380 TEAD1 are bridge molecules connecting Hippo-YAP pathway with CEBPβ, one of the core
381 adipogenesis regulators.

382 YAP/TAZ, TEADs and VGLLs are three categories of crucial transcriptional effectors of
383 the Hippo-YAP pathway. YAP/TAZ interacts with TEADs to regulate target gene expression,
384 and VGLLs function as suppressors of YAP/TEAD1 complex by competing for TEAD (Koontz
385 et al., 2013). Published data show that YAP and TAZ suppress BAT lipogenesis, because
386 reducing YAP and TAZ expression in BAT robustly increased BAC lipid content. In the same
387 work, YAP and TAZ were found to serve as mechanosensor proteins in BAT to regulate BAC
388 thermogenesis. Mechanistically, adrenergic stimulation increases cytosolic $Ca^{2+}$ that activates
389 actomyosin machinery to cause cellular tension, which in turn increases *Ucp1* expression by
390 activating YAP/TAZ-TEAD complex (Tharp et al., 2018). In the current study, our data suggest

391 that VGLL4 has dual roles in the regulation of BAT development: during embryo development,
392 VGLL4 is required for brown preadipocytes differentiating into UCP1 positive brown
393 adipocytes and may regulate adipogenesis by preserving CEBPβ transcriptional activity; from
394 neonate to adulthood, VGLL4 favors lipogenesis and suppresses *Ucp1* expression, and
395 VGLL4 fulfills this function by competing against YAP/TAZ for limited TEAD proteins.

396 Although UCP1-dependent energy dissipation is critical for BAT thermogenesis
397 (Fedorenko et al., 2012), it is not the only molecular mechanism for BAT to generate heat.
398 UCP1-independent energy dissipation molecular mechanisms, such as
399 Ryr1-mediated $Ca^{2+}$ leak (Bal et al., 2012), also contribute to BAT thermogenesis. Different
400 from YAP/TAZ promoting BAT thermogenesis by increasing UCP1 expression, VGLL4
401 induction of adult BAT thermogenesis is associated with *Ucp1* down-regulation, thus
402 suggesting that VGLL4 increases BAT thermogenesis by activating UCP1-independent
403 energy dissipation mechanisms. Since *Casq1* encodes a $Ca^{2+}$ buffer protein and it is up-
404 regulated by VGLL4, future studies are required to test whether VGLL4 promotes
405 thermogenesis through activating futile $Ca^{2+}$ recycling (Guarnieri et al., 2022).

406 In conclusion, our data suggest that Hippo-YAP pathway terminal effector proteins (e.g.,
407 TEAD1 and VGLL4) regulate BAT adipogenesis through modulating the transcriptional activity
408 of CEBPβ, thus improving our understanding of how Hippo-YAP pathway regulates BAT
409 development and function.

410 **Materials and Methods**

411 Refer to the Supplemental Information for Extended Materials and Methods.

412 *Mice*

413 All animal procedures were approved by the Institutional Animal Care and Use
414 Committee of the Masonic Medical Research Institute. Wild type C57/BL6J mice were used in
415 this study. C57/BL6J mice were originally purchased from Jackson Laboratory and maintained
416 in the AAALAC accredited (#001865) mouse facility of Masonic Medical Research Institute

417 (MMRI). *Vgll4* knockout mouse line *(Sheldon et al., 2022), Tead1*$^{fb}$ knockin (Lin et al., 2016)
418 and BirA mouse lines were published previously (Driegen et al., 2005).

419 *Immortalized brown preadipocyte (IBA) cell line culture and differentiation*

420 IBA cells were a gift of Dr. Deplancke from Swiss Institute of Bioinformatics. IBAs were
421 cultured in DMEM with 10% FBS and antibiotics, maintained at less than 80% confluence
422 before passaging. Differentiation of IBAs and maintenance of differentiated IBA cells were
423 achieved following a published protocol (Pradhan et al., 2017). To test the effects of VGLL4,
424 adenovirus harboring VGLL4 was added into the IBAs at a dose of 20 multiplicity of infection
425 (MOI) before differentiation. Cells were fixed and stained with Oil Red O six days after
426 differentiation.

427 *RNA-seq and data analysis*

428 Total RNA was extracted from the brown adipose tissue of P0 pups using PureLink RNA
429 Mini Kit (Thermo Fisher, 12183020). Polyadenylated RNA from 2 μg total RNA was
430 subsequently purified using Oligo(dT) Dynabeads (Thermo Fisher, 61005). RNA-seq libraries
431 were prepared with ScriptSeq V2 RNA-seq library kit (Illumina, SSV21124). Single-end reads
432 were sequenced using a NextSeq500 sequencer. RNA-seq reads were aligned to mm9 by
433 Tophat (Trapnell et al., 2009) and read counts were calculated by Htseq-count (Anders et al.,
434 2015). DEseq (Anders and Huber, 2010) was next used to perform statistical analysis of
435 differential gene expression. An adjusted P-value of 0.05 was used as cutoff to identify
436 differentially regulated genes.

437 *Histology and immunostaining*

438 Brown adipose tissue and inguinal white adipose tissue were fixed in 4% PFA,
439 cryoprotected with 30% sucrose, and embedded in OCT. 10 μm sections were used for Oil
440 Red O staining. H&E staining was performed on paraffin-embedded sections. Immunostaining
441 was performed on cryosections and detected with Alexa-labelled secondary antibodies
442 (Invitrogen). Antibody sources are listed in Supplementary Table 2. EdU was administered

443 intraperitoneally at 200 µg (pregnant dams), 2 hours before tissue collection. EdU was
444 detected with Click-iT chemistry (Invitrogen). Imaging was performed on a Keyence BZ-X800
445 microscopy system.

446 *Tead1 bioChIP-seq of interscapular brown adipose tissues*

447 Tead1 bioChIP-seq was performed as described previously (Akerberg et al., 2019). Briefly,
448 interscapular brown adipose tissues of postnatal day 0 (P0) were harvested. Tissues from 3-4
449 mice were pooled as one sample, and homogenized with a motor-driven disperser, and then
450 crosslinked in 1% formaldehyde in PBS for 10 minutes at room temperature and subsequently
451 quenched with 125 mM glycine for 5 min. Chromatin was fragmented using a microtip
452 sonicator (Qsonica, S-3000) at 70% amplitude for 8 minutes. Biotinylated Tead1 and bound
453 chromatin was pulled down by incubation with streptavidin beads (ThermoFisher Scientific,
454 11206D). Bead-bound chromatin was resuspended in SDS elution buffer (50 mM Tris–HCl pH
455 8,10 mM EDTA, 1% SDS) and incubated overnight at 65 °C to reverse crosslinking. After
456 RNAse A and Proteinase K treatment, ChIP DNA was purified using Qiagen MinElute
457 columns. Libraries were constructed using the KAPA HyperPrep ChIP-seq library preparation
458 kit (Roche, cat# 07962347001). Sequencing (75 nt single end) was performed on an Illumina
459 NextSeq 500.

460 *Tead1 bioChIP-seq data analysis*

461 The raw reads from two biological replicate bioChIP-Seq datasets were mapped to the Mus
462 musculus genome (mm9 build) using Bowtie (Langmead et al., 2009) (Ref_Langmead).
463 Alignments with more than one match were removed. MACS2 (Zhang et al., 2008) was used
464 to determine peaks in each replicate with p-value 1e-5 as cutoff. The peak list was further
465 filtered to remove all blacklisted regions. The intersection of peaks from the replicates yielded
466 the reproducible peaks. The intersection and union sets were determined by the Bedtools
467 (Quinlan and Hall, 2010) intersect function. The enriched motifs were determined with Homer
468 de novo motif algorithm analysis (Heinz et al., 2010).

469 *Statistics*

470 Data values (e.g., gene and protein expression data) were expressed as mean ± SD.
471 Normally distributed data were analyzed with student's t-test (two groups) or one-way ANOVA
472 followed by Tukey's post hoc test (more than two groups). Non-parametric data (e.g., cell
473 size) were analyzed using Mann-Whitney test (two groups). Prism10 software was used to
474 plot the bar/violin graphs and to perform the statistical analysis.

475 **Data availability**

476 TEAD1 bioChIP-seq data of postnatal day 0 (P0) mouse brown adipose tissue has been
477 deposited to gene expression omnibus GSE271532. Bulk RNA-seq data of wildtype and Vgll4
478 knockout P0 mouse brown adipose tissue has been deposited to GSE271533.

479 **Sources of Funding**

480 Z. Lin was supported by AHA Scientist Development Grant 15SDG25590001, NIH
481 HL138454-01, and 1R01HL146810. W.T. Pu was supported by NIH R01HL116461 and
482 R01HL146634.

483 **Author contributions:** Z.L. designed and interpreted the study. P.Z., C.W.K. and Z.L. per-
484 formed experiments with the help from A.D., G. W. and S.N. F. G. analyzed the BAT RNA-seq
485 data. B. D. provided the IBA RNA-seq data and IBA cell line. P. Z., C.W.K. W.T. P and Z. L an-
486 alyzed the results. Z.L wrote the manuscript. C.W.K. and W.T. P. revised the manuscript.

487 **Acknowledgment:** We thank Justkin King and Jimiao Sun from Boston Children's Hospital
488 for quantifying the mouse pups lipid content with the magnetic resonance imaging (MRI) data.

489 **Disclosures.** Z.L. holds a patent (Patent No. US 11,319, 354 B2) that is related with the cur-
490 rent study.

## References:


Akerberg BN, Gu F, VanDusen NJ, Zhang X, Dong R, Li K, Zhang B, Zhou B, Sethi I, Ma Q, Wasson L, Wen T, Liu J, Dong K, Conlon FL, Zhou J, Yuan GC, Zhou P, Pu WT. 2019. A reference map of murine cardiac transcription factor chromatin occupancy identifies dynamic and conserved enhancers. *Nat Commun* **10**: 4907.

An Y, Kang Q, Zhao Y, Hu X, Li N. 2013. Lats2 modulates adipocyte proliferation and differentiation via hippo signaling. *PLoS One* **8**: e72042.

Anders S, Huber W. 2010. Differential expression analysis for sequence count data. *Genome Biol* **11**: R106.

Anders S, Pyl PT, Huber W. 2015. HTSeq--a Python framework to work with high-throughput sequencing data. *Bioinformatics* **31**: 166–169.

Anthony SR, Guarnieri A, Lanzillotta L, Gozdiff A, Green LC, O'Grady K, Helsley RN, Owens Iii AP, Tranter M. 2020. HuR expression in adipose tissue mediates energy expenditure and acute thermogenesis independent of UCP1 expression. *Adipocyte* **9**: 335–345.

Bal NC, Maurya SK, Sopariwala DH, Sahoo SK, Gupta SC, Shaikh SA, Pant M, Rowland LA, Bombardier E, Goonasekera SA. 2012. Sarcolipin is a newly identified regulator of muscle-based thermogenesis in mammals. *Nature medicine* **18**: 1575–1579.

Bégay V, Baumeier C, Zimmermann K, Heuser A, Leutz A. 2018. The C/EBPβ LIP isoform rescues loss of C/EBPβ function in the mouse. *Sci Rep* **8**: 8417.

Cypess AM, Kahn CR. 2010. Brown fat as a therapy for obesity and diabetes. *Curr Opin Endocrinol Diabetes Obes* **17**: 143–149.

Cypess AM, Lehman S, Williams G, Tal I, Rodman D, Goldfine AB, Kuo FC, Palmer EL, Tseng YH, Doria A, Kolodny GM, Kahn CR. 2009. Identification and importance of brown adipose tis-

514 sue in adult humans. *N Engl J Med* **360**: 1509–1517.

515 Driegen S, Ferreira R, van Zon A, Strouboulis J, Jaegle M, Grosveld F, Philipsen S, Meijer D.
516 2005. A generic tool for biotinylation of tagged proteins in transgenic mice. *Transgenic re-*
517 *search* **14**: 477–482.

518 Farmer SR. 2006. Transcriptional control of adipocyte formation. *Cell Metab* **4**: 263–273.

519 Fedorenko A, Lishko PV, Kirichok Y. 2012. Mechanism of fatty-acid-dependent UCP1 uncou-
520 pling in brown fat mitochondria. *Cell* **151**: 400–413.

521 Ge SX, Jung D, Yao R. 2020. ShinyGO: a graphical gene-set enrichment tool for animals and
522 plants. *Bioinformatics* **36**: 2628–2629.

523 Gesta S, Tseng YH, Kahn CR. 2007. Developmental origin of fat: tracking obesity to its
524 source. *Cell* **131**: 242–256.

525 Giralt M, Villarroya F. 2013. White, brown, beige/brite: different adipose cells for different func-
526 tions. *Endocrinology* **154**: 2992–3000.

527 Greenberg AS, Egan JJ, Wek SA, Garty NB, Blanchette-Mackie EJ, Londos C. 1991. Perilipin,
528 a major hormonally regulated adipocyte-specific phosphoprotein associated with the periphery
529 of lipid storage droplets. *J Biol Chem* **266**: 11341–11346.

530 Guarnieri AR, Benson TW, Tranter M. 2022. Calcium cycling as a mediator of thermogenic
531 metabolism in adipose tissue. *Mol Pharmacol* **102**: 51–59.

532 Guo L, Li X, Tang QQ. 2015. Transcriptional regulation of adipocyte differentiation: a central
533 role for CCAAT/enhancer-binding protein (C/EBP) β. *J Biol Chem* **290**: 755–761.

534 Heaton JM. 1972. The distribution of brown adipose tissue in the human. *J Anat* **112**: 35–39.

535 Heinz S, Benner C, Spann N, Bertolino E, Lin YC, Laslo P, Cheng JX, Murre C, Singh H,
536 Glass CK. 2010. Simple combinations of lineage-determining transcription factors prime cis-

537 regulatory elements required for macrophage and B cell identities. *Mol Cell* **38**: 576–589.

538 Hiraike Y, Waki H, Yu J, Nakamura M, Miyake K, Nagano G, Nakaki R, Suzuki K, Kobayashi
539 H, Yamamoto S, Sun W, Aoyama T, Hirota Y, Ohno H, Oki K, Yoneda M, White AP, Tseng YH,
540 Cypess AM, Larsen TJ, Jespersen NZ, Scheele C, Tsutsumi S, Aburatani H, Yamauchi T, Kad-
541 owaki T. 2017. NFIA co-localizes with PPARγ and transcriptionally controls the brown fat gene
542 program. *Nat Cell Biol* **19**: 1081–1092.

543 Jimenez V, Muñoz S, Casana E, Mallol C, Elias I, Jambrina C, Ribera A, Ferre T, Franck-
544 hauser S, Bosch F. 2013. In vivo adeno-associated viral vector-mediated genetic engineering
545 of white and brown adipose tissue in adult mice. *Diabetes* **62**: 4012–4022.

546 Jones JR, Barrick C, Kim KA, Lindner J, Blondeau B, Fujimoto Y, Shiota M, Kesterson RA,
547 Kahn BB, Magnuson MA. 2005. Deletion of PPARgamma in adipose tissues of mice protects
548 against high fat diet-induced obesity and insulin resistance. *Proc Natl Acad Sci U S A* **102**:
549 6207–6212.

550 Kim JI, Park J, Ji Y, Jo K, Han SM, Sohn JH, Shin KC, Han JS, Jeon YG, Nahmgoong H, Han
551 KH, Kim J, Kim S, Choe SS, Kim JB. 2019. During Adipocyte Remodeling, Lipid Droplet Con-
552 figurations Regulate Insulin Sensitivity through F-Actin and G-Actin Reorganization. *Mol Cell*
553 *Biol* **39**: e00210–19.

554 Koontz LM, Liu-Chittenden Y, Yin F, Zheng Y, Yu J, Huang B, Chen Q, Wu S, Pan D. 2013.
555 The Hippo effector Yorkie controls normal tissue growth by antagonizing scalloped-mediated
556 default repression. *Dev Cell* **25**: 388–401.

557 Langmead B, Trapnell C, Pop M, Salzberg SL. 2009. Ultrafast and memory-efficient alignment
558 of short DNA sequences to the human genome. *Genome biology* **10**: 1–10.

559 Lin Z, Guo H, Cao Y, Zohrabian S, Zhou P, Ma Q, VanDusen N, Guo Y, Zhang J, Stevens SM,
560 Liang F, Quan Q, van Gorp PR, Li A, Dos Remedios C, He A, Bezzerides VJ, Pu WT. 2016.

561 Acetylation of VGLL4 Regulates Hippo-YAP Signaling and Postnatal Cardiac Growth. *Dev*
562 *Cell* **39**: 466–479.

563 Lin Z, Zhou P, von Gise A, Gu F, Ma Q, Chen J, Guo H, van Gorp PR, Wang DZ, Pu WT.
564 2015. Pi3kcb links Hippo-YAP and PI3K-AKT signaling pathways to promote cardiomyocyte
565 proliferation and survival. *Circ Res* **116**: 35–45.

566 Manchado C, Yubero P, Viñas O, Iglesias R, Villarroya F, Mampel T, Giralt M. 1994. CCAAT/
567 enhancer-binding proteins α and β in brown adipose tissue: evidence for a tissue-specific pat-
568 tern of expression during development. *Biochemical Journal* **302**: 695–700.

569 Meng Z, Moroishi T, Guan KL. 2016. Mechanisms of Hippo pathway regulation. *Genes Dev*
570 **30**: 1–17.

571 Mitchell NS, Catenacci VA, Wyatt HR, Hill JO. 2011. Obesity: overview of an epidemic. *Psy-*
572 *chiatr Clin North Am* **34**: 717–732.

573 Morrison S, McGee SL. 2015. 3T3-L1 adipocytes display phenotypic characteristics of multi-
574 ple adipocyte lineages. *Adipocyte* **4**: 295–302.

575 Negron SG, Ercan-Sencicek AG, Freed J, Walters M, Lin Z. 2020. Both proliferation and lipo-
576 genesis of brown adipocytes contribute to postnatal brown adipose tissue growth in mice. *Sci*
577 *Rep* **10**: 20335.

578 Ovcharenko I, Nobrega MA, Loots GG, Stubbs L. 2004. ECR Browser: a tool for visualizing
579 and accessing data from comparisons of multiple vertebrate genomes. *Nucleic Acids Res* **32**:
580 W280–6.

581 Pan D. 2010. The hippo signaling pathway in development and cancer. *Dev Cell* **19**: 491–505.

582 Park BH, Kim DS, Won GW, Jeon HJ, Oh BC, Lee Y, Kim EG, Lee YH. 2012. Mammalian
583 ste20-like kinase and SAV1 promote 3T3-L1 adipocyte differentiation by activation of PPARγ.

*PLoS One* **7**: e30983.

Patel R, Santoro A, Hofer P, Tan D, Oberer M, Nelson AT, Konduri S, Siegel D, Zechner R, Saghatelian A, Kahn BB. 2022. ATGL is a biosynthetic enzyme for fatty acid esters of hydroxy fatty acids. *Nature* **606**: 968–975.

Pradhan RN, Bues JJ, Gardeux V, Schwalie PC, Alpern D, Chen W, Russeil J, Raghav SK, Deplancke B. 2017. Dissecting the brown adipogenic regulatory network using integrative genomics. *Sci Rep* **7**: 42130.

Quinlan AR, Hall IM. 2010. BEDTools: a flexible suite of utilities for comparing genomic features. *Bioinformatics* **26**: 841–842.

Sanchez EJ, Lewis KM, Danna BR, Kang C. 2012. High-capacity Ca2+ binding of human skeletal calsequestrin. *J Biol Chem* **287**: 11592–11601.

Schulz TJ, Huang P, Huang TL, Xue R, McDougall LE, Townsend KL, Cypess AM, Mishina Y, Gussoni E, Tseng YH. 2013. Brown-fat paucity due to impaired BMP signalling induces compensatory browning of white fat. *Nature* **495**: 379–383.

Seale P, Kajimura S, Spiegelman BM. 2009. Transcriptional control of brown adipocyte development and physiological function--of mice and men. *Genes Dev* **23**: 788–797.

Seale P, Kajimura S, Yang W, Chin S, Rohas LM, Uldry M, Tavernier G, Langin D, Spiegelman BM. 2007. Transcriptional control of brown fat determination by PRDM16. *Cell Metab* **6**: 38–54.

Shearin AL, Monks BR, Seale P, Birnbaum MJ. 2016. Lack of AKT in adipocytes causes severe lipodystrophy. *Molecular metabolism* **5**: 472–479.

Sheldon C, Farley A, Ma Q, Pu WT, Lin Z. 2022. Depletion of VGLL4 Causes Perinatal Lethality without Affecting Myocardial Development. *Cells* **11**: 2832.

607 Subramanian A, Tamayo P, Mootha VK, Mukherjee S, Ebert BL, Gillette MA, Paulovich A,
608 Pomeroy SL, Golub TR, Lander ES, Mesirov JP. 2005. Gene set enrichment analysis: a
609 knowledge-based approach for interpreting genome-wide expression profiles. *Proc Natl Acad*
610 *Sci U S A* **102**: 15545–15550.

611 Symonds ME. 2013. Brown adipose tissue growth and development. *Scientifica (Cairo)* **2013**:
612 305763.

613 Tanaka T, Yoshida N, Kishimoto T, Akira S. 1997. Defective adipocyte differentiation in mice
614 lacking the C/EBPbeta and/or C/EBPdelta gene. *EMBO J* **16**: 7432–7443.

615 Tharp KM, Kang MS, Timblin GA, Dempersmier J, Dempsey GE, Zushin PH, Benavides J,
616 Choi C, Li CX, Jha AK, Kajimura S, Healy KE, Sul HS, Saijo K, Kumar S, Stahl A. 2018. Acto-
617 myosin-Mediated Tension Orchestrates Uncoupled Respiration in Adipose Tissues. *Cell*
618 *Metab* **27**: 602–615.e4.

619 Timmons JA, Wennmalm K, Larsson O, Walden TB, Lassmann T, Petrovic N, Hamilton DL,
620 Gimeno RE, Wahlestedt C, Baar K, Nedergaard J, Cannon B. 2007. Myogenic gene expres-
621 sion signature establishes that brown and white adipocytes originate from distinct cell lin-
622 eages. *Proc Natl Acad Sci U S A* **104**: 4401–4406.

623 Townsend K, Tseng YH. 2012. Brown adipose tissue: Recent insights into development, meta-
624 bolic function and therapeutic potential. *Adipocyte* **1**: 13–24.

625 Trapnell C, Pachter L, Salzberg SL. 2009. TopHat: discovering splice junctions with RNA-Seq.
626 *Bioinformatics* **25**: 1105–1111.

627 Xin M, Kim Y, Sutherland LB, Qi X, McAnally J, Schwartz RJ, Richardson JA, Bassel-Duby R,
628 Olson EN. 2011. Regulation of insulin-like growth factor signaling by Yap governs cardiomy-
629 ocyte proliferation and embryonic heart size. *Sci Signal* **4**: ra70.

630 Xiong W, Zhao X, Villacorta L, Rom O, Garcia-Barrio MT, Guo Y, Fan Y, Zhu T, Zhang J, Zeng

631 R. 2018. Brown adipocyte-specific PPARγ (peroxisome proliferator-activated receptor γ) dele-
632 tion impairs perivascular adipose tissue development and enhances atherosclerosis in mice.
633 *Arteriosclerosis, thrombosis, and vascular biology* **38**: 1738–1747.

634 Yao X, Shan S, Zhang Y, Ying H. 2011. Recent progress in the study of brown adipose tissue.
635 *Cell Biosci* **1**: 35.

636 Yore MM, Syed I, Moraes-Vieira PM, Zhang T, Herman MA, Homan EA, Patel RT, Lee J,
637 Chen S, Peroni OD, Dhaneshwar AS, Hammarstedt A, Smith U, McGraw TE, Saghatelian A,
638 Kahn BB. 2014. Discovery of a class of endogenous mammalian lipids with anti-diabetic and
639 anti-inflammatory effects. *Cell* **159**: 318–332.

640 Yu FX, Zhang Y, Park HW, Jewell JL, Chen Q, Deng Y, Pan D, Taylor SS, Lai ZC, Guan KL.
641 2013. Protein kinase A activates the Hippo pathway to modulate cell proliferation and differen-
642 tiation. *Genes Dev* **27**: 1223–1232.

643 Zhang W, Xu J, Li J, Guo T, Jiang D, Feng X, Ma X, He L, Wu W, Yin M, Ge L, Wang Z, Ho
644 MS, Zhao Y, Fei Z, Zhang L. 2018. The TEA domain family transcription factor TEAD4 re-
645 presses murine adipogenesis by recruiting the cofactors VGLL4 and CtBP2 into a transcriptio-
646 nal complex. *J Biol Chem* **293**: 17119–17134.

647 Zhang Y, Liu T, Meyer CA, Eeckhoute J, Johnson DS, Bernstein BE, Nusbaum C, Myers RM,
648 Brown M, Li W, Liu XS. 2008. Model-based analysis of ChIP-Seq (MACS). *Genome Biol* **9**:
649 R137.

650 Zimmermann R, Strauss JG, Haemmerle G, Schoiswohl G, Birner-Gruenberger R, Riederer
651 M, Lass A, Neuberger G, Eisenhaber F, Hermetter A, Zechner R. 2004. Fat mobilization in adi-
652 pose tissue is promoted by adipose triglyceride lipase. *Science* **306**: 1383–1386.

653 Zwick RK, Guerrero-Juarez CF, Horsley V, Plikus MV. 2018. Anatomical, Physiological, and
654 Functional Diversity of Adipose Tissue. *Cell Metab* **27**: 68–83.

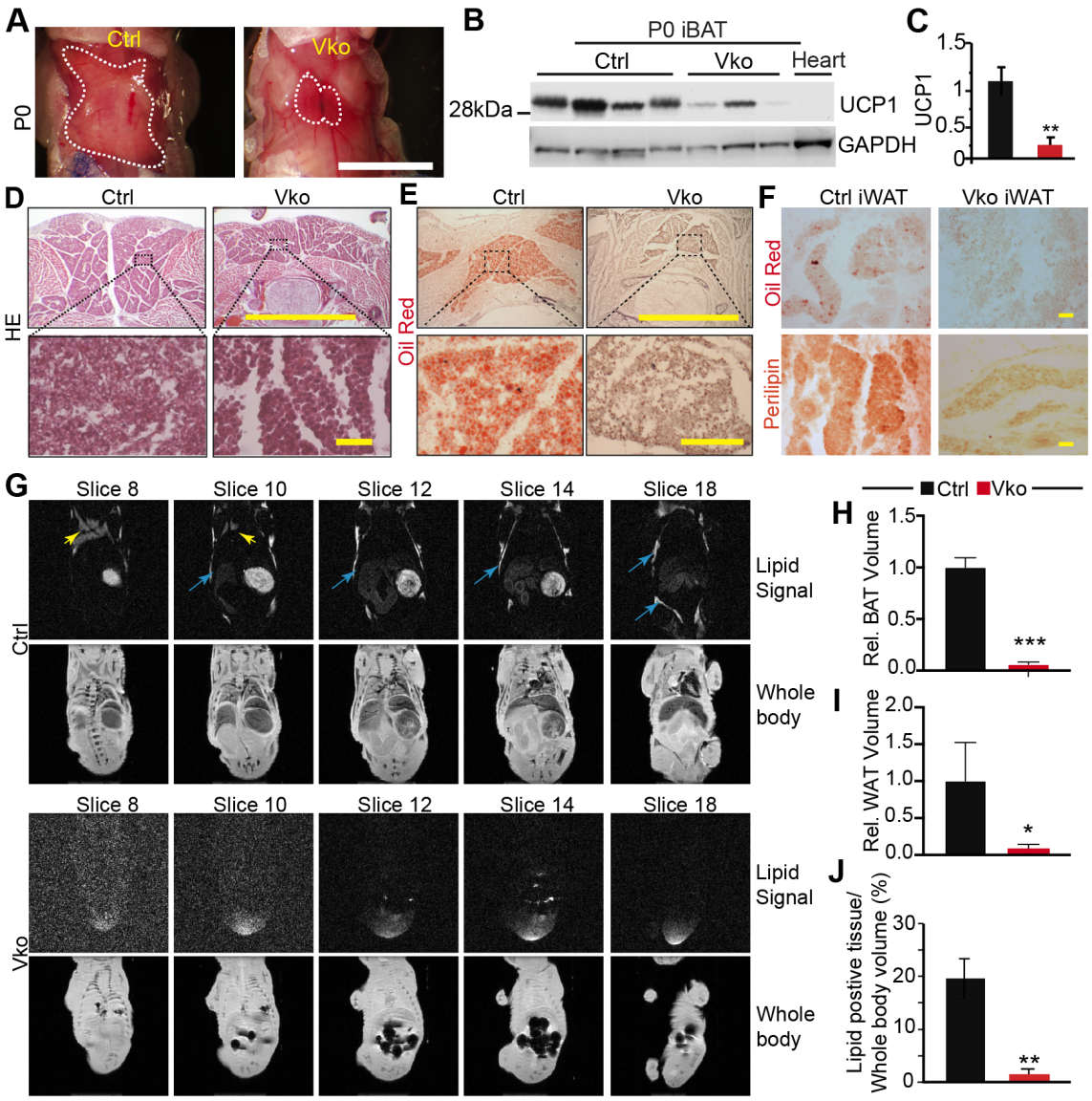


**Figure 1. Classical brown adipose tissue growth requires VGLL4.**

**A**. Gross morphology of classical interscapular brown adipose tissue at P0. Dotted lines indicate the BAT depot. Scale bar=4 mm. **B**. UCP1 immunoblot with P0 BAT protein. Heart protein was used as negative control. **C**. Densitometry quantification of UCP1. Protein levels were normalized to GAPDH. N=4. Student's t test, **, P<0.01. **D**. HE staining of BAT. Top panel, scale bar =4 mm; bottom panel, scale bar=50 μm. **E.** Oil Red O staining of BAT. Top panel, bar= 4 mm; bottom panel, scale bar=1 mm. **F.** Oil Red O staining and Perilipin immunohistological staining of iWAT. Scale bar = 50 μm **G**. Visualization of whole body trunk for lipid content by a series of MRI images using P0 mouse pups. Water signal was

**Figure 1. Classical brown adipose tissue growth requires VGLL4.**

suppressed in the lipid only images. Blue and yellow arrows indicate BAT and and subcutaneous WAT, respectively. **H.** BAT lipid content comparison. **I**. WAT lipid content comparison. **J**. Quantification of the total lipid content. The percentage was calculated by normalizing the lipid positive tissue volume to the body trunk volume. Student t-test: *P<0.05, n=4.

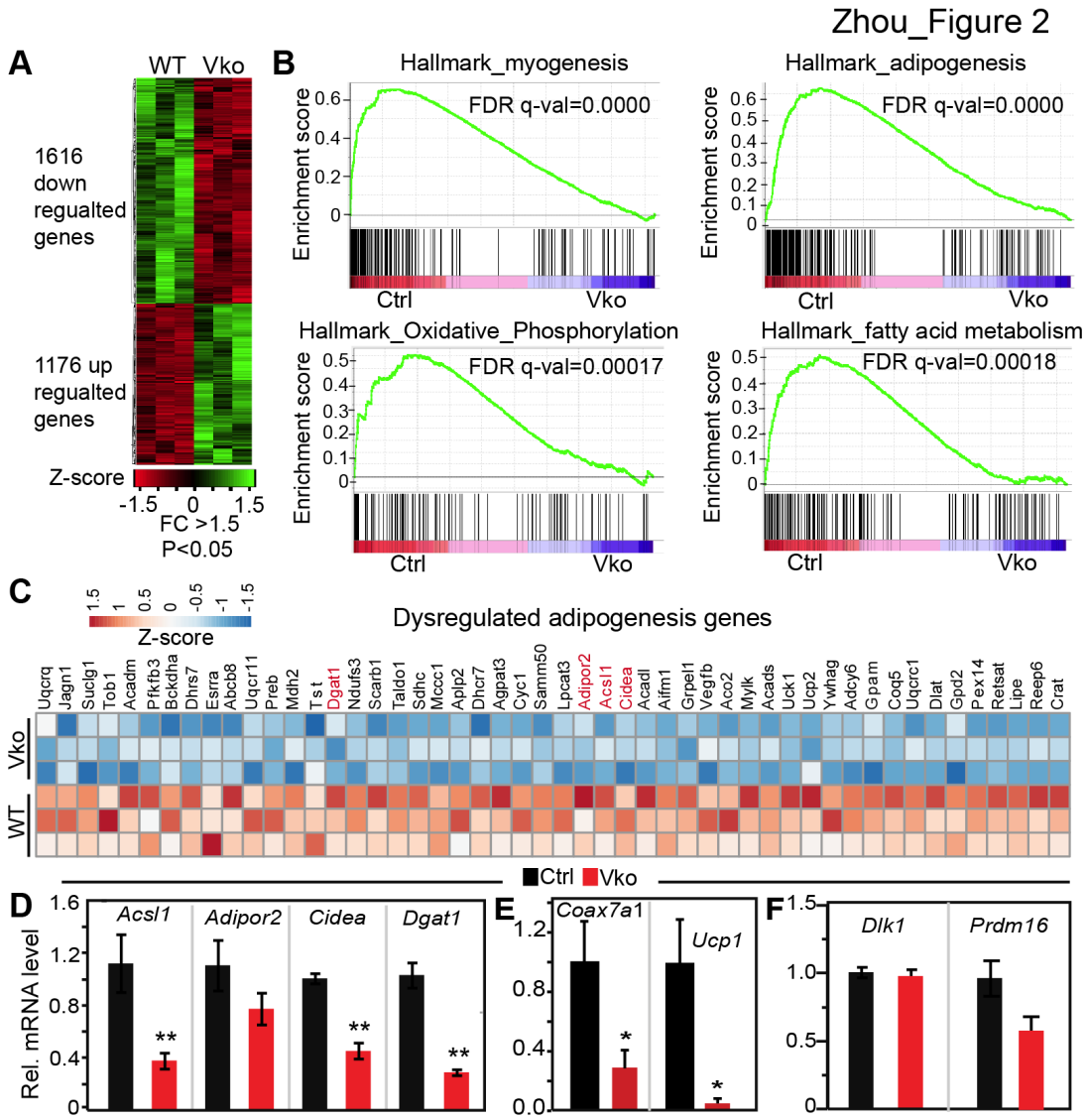


**Figure 2. Loss of VGLL4 disrupts the adipogenesis gene expression program of BAT.**

**A**. Heat map of differentially expressed genes (DEG). RNA sequencing data from P0 BAT was analyzed with Deseq. N=3. **B**. Gene set enrichment analysis (GESA). GESA was carried out with the Deseq2-derived gene expression data set. The top four gene sets enriched in wild-type BAT were shown. **C**. A heat map of differentially expressed fatty acid metabolism/ adipogenesis genes. **D**. qRT-PCR validation of selected lipogenesis genes dysregulated in *Vko* BAT. **E-F.** qRT-PCR measurement of brown adipocyte differentiation-related genes. D, E and F, N=5. Student t-test, *, P<0.05. All the tested mRNAs were normalized by endogenous 36B4 mRNA.

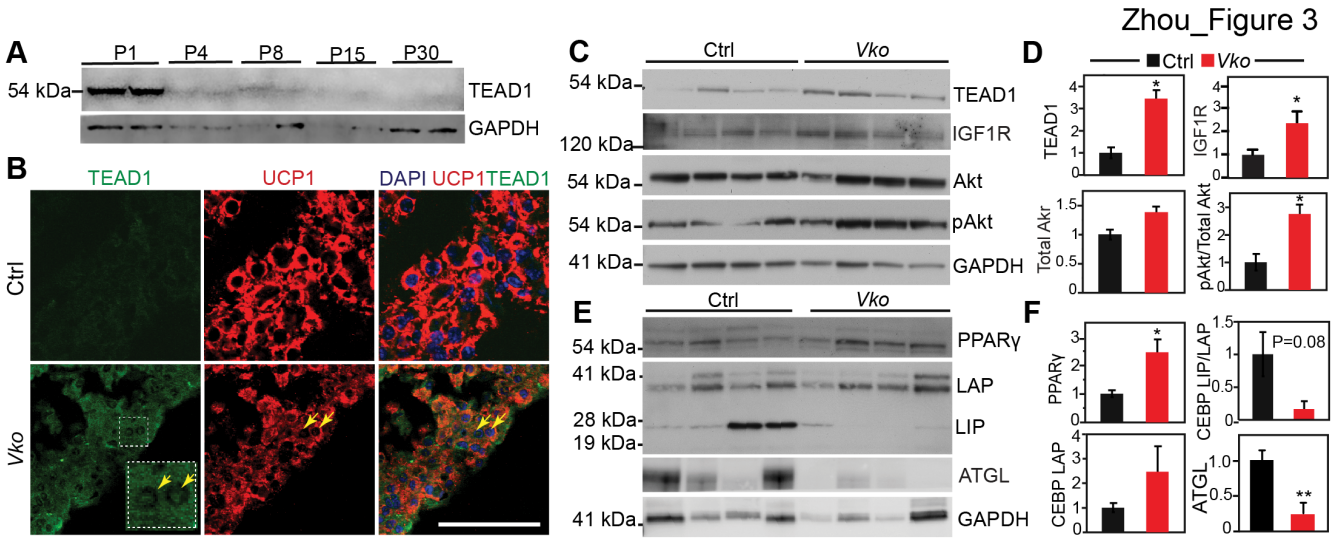


**Figure 3. Loss of VGLL4 activates TEAD1. A.** Western blot analysis of TEAD1 expression in BAT. BAT proteins collected from mice of different ages were compared by western blot. GAPDH was used as loading control. **B**. Immunofluorescence images of UCP1 and TEAD1 stained BAT sections. Yellow arrows indicate brown adipocytes enriched with nuclear TEAD1. Scale bar = 50 μm. **C**. Western blot analysis of TEAD1 and the crucial IGF1-Akt pathway components. **D**. Densitometry quantification of TEAD1, IGF1R, total Akt and phosphorylated Akt. **E**. Western blot analysis of crucial adipogenesis regulators. **F**. Densitometry quantification of PPARγ, C-LAP, C-LIP and ATGL. P0 interscapular BAT protein was used for western blots. D and F, protein levels were normalized to GAPDH. N=4. Student's t test, *, P<0.05; **, P<0.01.

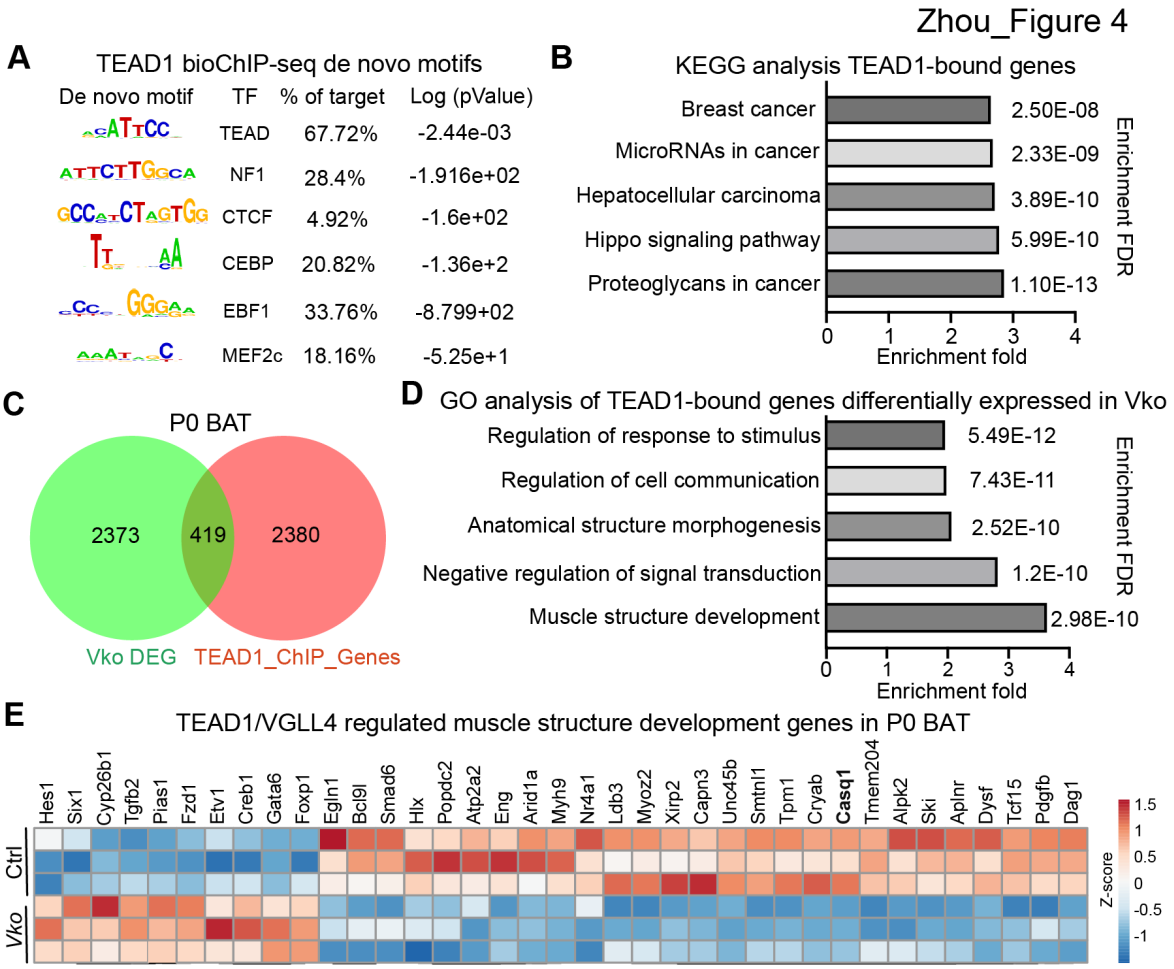


**Figure 4. Identification of VGLL4/TEAD1 target genes in BAT. A**. De novo motif discovery analysis within the identified TEAD1 binding sites. P0 BAT was used for TEAD1 ChIP seq. **B**. KEGG analysis of TEAD1 bound genes. The bar graph shows the top five enriched signaling pathways. **C**. Venn diagram showing the relationship between TEAD1 bound genes and differentially expressed genes in *Vko* (*Vko* DEG) brown adipose tissue. **D**. Gene Ontology analysis of the TEAD1/VGLL4 target genes. The 419 genes both dysregulated in *Vko* and bound by TEAD1 were applied to Shiny GO analysis. The top 5 enriched biological processes are listed in the bar graph. **E.** Heat map of differentially expressed VGLL4/TEAD1 regulated myogenic genes. RNA sequencing data from P0 BAT were presented. N=3.

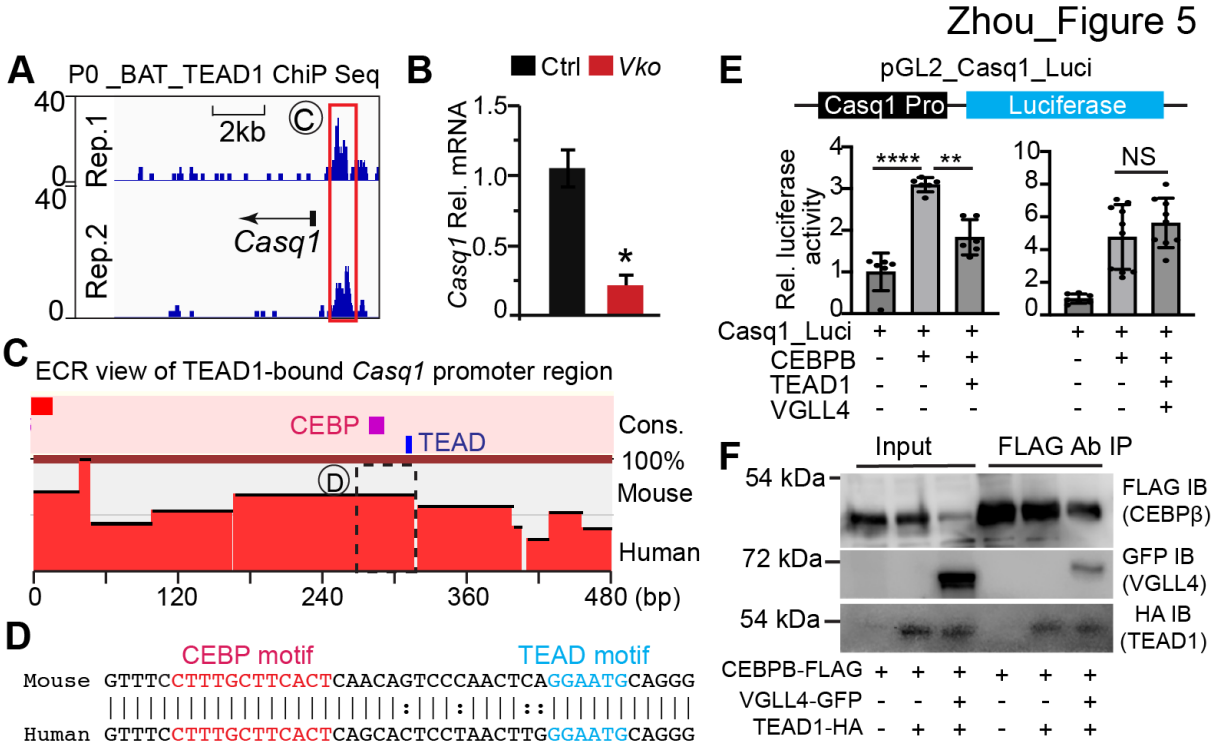


**Figure 5. VGLL4 alleviates TEAD1 suppression of CEBP transcriptional activity.**

**A**. Genome browser view showing ChIP-seq of TEAD1 occupancy near the transcriptional start site (TSS) or *Casq1*. ChIP-seq data from two biological replicates are shown. **B.** qRT-PCR measurement of *Casq1*. P0 control and *Vko* BAT mRNA was used for qRT-PCR analysis. All the tested mRNAs were normalized by endogenous 36B4 mRNA. N=4. Student t-test, *, P<0.05. **C**. Evolutionary conservation of genomes (ECR) browser view of the TEAD1-bound *Casq1* promoter region. **D**. Alignment of the mouse and human *Casq1* promoter sequences enclosed by dotted rectangle in C. Conserved CEBP and TEAD binding motifs are highlighted. **E**. Luciferase reporter assay. The TEAD1-bound *Casq1* promoter sequence was cloned into pGL2 to generate Caqs1_Luci reporter plasmid. Indicated plasmids were transfected into HEK293T cells and *Casq1* promoter activity was measured by dual-luciferase assay. N=6. One-way ANOVA followed by multiple comparison analysis, ****, p<0.0001; ***, p<0.001. **F**. Co-immunoprecipitation (Co-IP) assay. Indicated plasmids were transfected into HEK293T cells. Flag antibody was used for Co-IP.

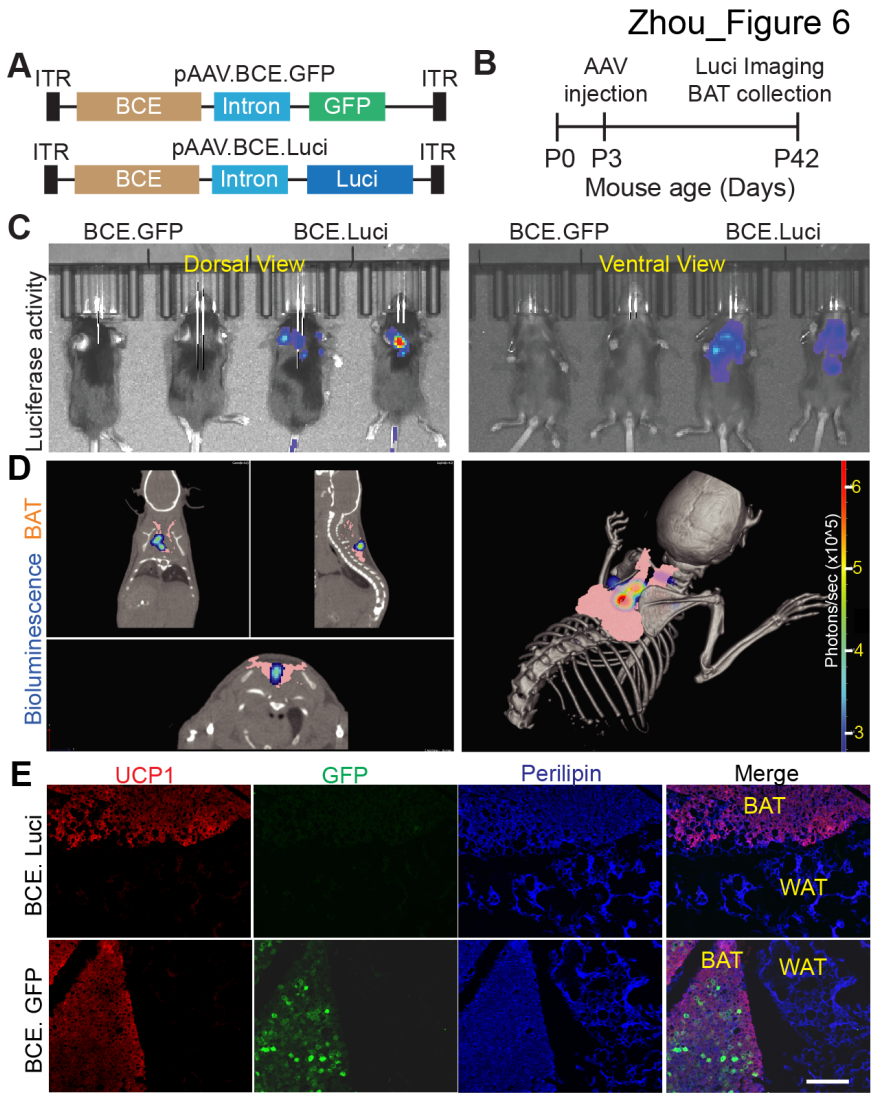


**Figure 6. AAV9.BCE specifically expresses cargo genes in brown adipocytes.**

**A**. Schematic representation of pAAV.BCE.Luci and pAAV.BCE.GFP construct. Luciferase or GFP gene was placed downstream of BCE. One chimera intron of human beta-globin and immunoglobulin heavy chain genes was placed between BCE and cargo genes to increase cargo gene expression. ITR: inverted terminal repeat sequence. **B**. Experimental design. AAV9.BCE.luci or AAV9.BCE.GFP was injected into 3 days old pups (P3) subcutaneously. At 42 days after birth (P42), bioluminescence activity was measured with PerkinElmer in vivo imaging system (IVIS). **C**. Representative bioluminescence images generated by IVIS system. Both dorsal and ventral views were presented. **D**. Representative coregistration of bioluminescence signal and *microCT* segmented interscapular brown adipose tissue from an

**Figure 6. AAV9.BCE specifically expresses cargo genes in brown adipocytes.**

AAV.BCE.Luci mouse highlights the origin of the biolumenscence signal within the BAT volume. Pink: brown adipose tissue. Rainbow, bioluminescence signal positive tissues.

**E**. Immunofluoresence images of BAT. BAT was collected at P42 and used for immunofluorescence staining. UCP1, BAT marker protein. Perilipin: adipose tissue marker (BAT and WAT) protein. Scale bar=200 μm

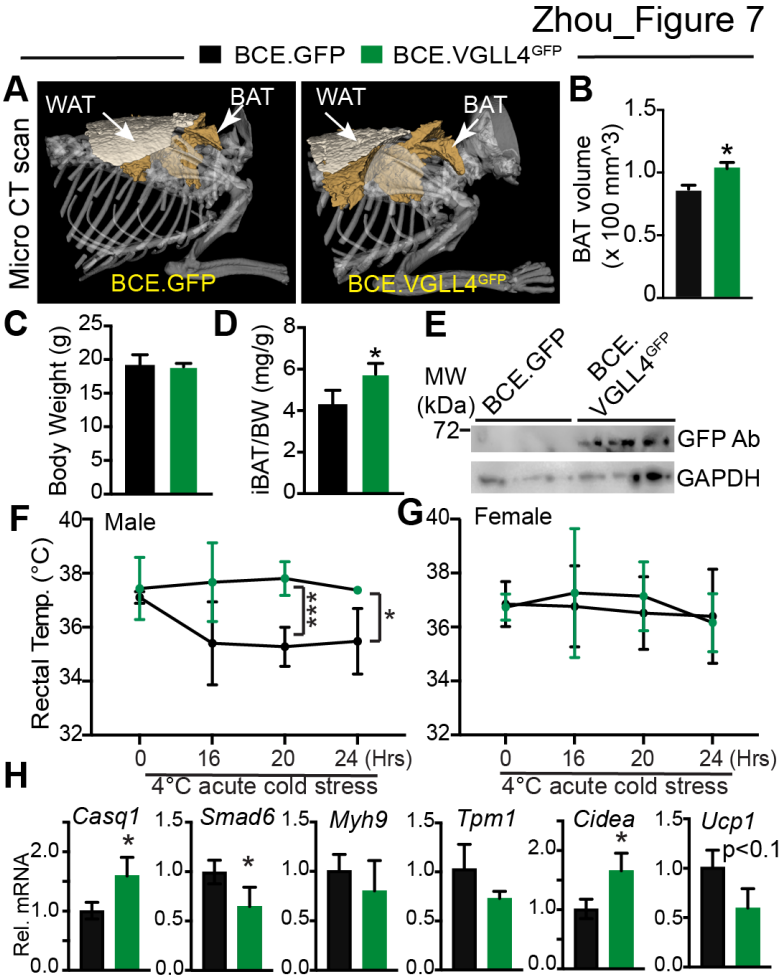


**Figure 7. AAV9.BCE.VGLL4 promotes BAT growth.** **A**. Representative volumetric images generated by microCT scan highlight the BAT (brown) and WAT (white) in the interscapular regions of the mice. Bones were labeled as grey. **B**. Quantification of BAT volume. **C.** Body weight. **D**. Interscapular BAT and body weight ratio. N=3. Student t-test, *, p<0.05. **E**. VGLL4 immunoblot with P42 BAT protein. GAPDH was used as internal control. **F-G.** Acute cold-stress test. BCE.GFP or BCE.VGLL4$^{GFP}$ was injected into 3 days old pups (P3) subcutaneously. At 42 days after birth (P42), mice were treated with acute cold stress (4°C) for 24 hours. E, male mice rectal temperature. BCE.GFP, n=4; BCE.VGLL4$^{GFP}$, n=3. Student t-test, ***, p<0.001; *, p<0.05. F, female mice core temperature, n=4 for each group. **H.** qRT-PCR measurement of gene expression. P42 BAT mRNA was used for qRT-PCR analysis. All the tested mRNAs were normalized by endogenous 36B4 mRNA. N=4. Student t-test, *, P<0.05.